

ARTICLE

DOI: 10.1038/s41467-017-01277-x

OPEN

Maximizing T_c by tuning nematicity and magnetism in $\text{FeSe}_{1-x}\text{S}_x$ superconductors

K. Matsuura¹, Y. Mizukami¹, Y. Arai¹, Y. Sugimura¹, N. Maejima², A. Machida², T. Watanuki², T. Fukuda³, T. Yajima⁴, Z. Hiroi⁴, K.Y. Yip⁵, Y.C. Chan⁵, Q. Niu⁵, S. Hosoi¹, K. Ishida¹, K. Mukasa¹, S. Kasahara⁶, J.-G. Cheng⁷, S.K. Goh⁵, Y. Matsuda⁶, Y. Uwatoko⁴ & T. Shibauchi¹

A fundamental issue concerning iron-based superconductivity is the roles of electronic nematicity and magnetism in realising high transition temperature (T_c). To address this issue, FeSe is a key material, as it exhibits a unique pressure phase diagram involving non-magnetic nematic and pressure-induced antiferromagnetic ordered phases. However, as these two phases in FeSe have considerable overlap, how each order affects superconductivity remains perplexing. Here we construct the three-dimensional electronic phase diagram, temperature (T) against pressure (P) and isovalent S-substitution (x), for $\text{FeSe}_{1-x}\text{S}_x$. By simultaneously tuning chemical and physical pressures, against which the chalcogen height shows a contrasting variation, we achieve a complete separation of nematic and antiferromagnetic phases. In between, an extended non-magnetic tetragonal phase emerges, where T_c shows a striking enhancement. The completed phase diagram uncovers that high- T_c superconductivity lies near both ends of the dome-shaped antiferromagnetic phase, whereas T_c remains low near the nematic critical point.

¹Department of Advanced Materials Science, University of Tokyo, Kashiwa, Chiba 277-8561, Japan. ²Synchrotron Radiation Research Center, National Institutes for Quantum and Radiological Science and Technology, Sayo, Hyogo 679-5148, Japan. ³Materials Sciences Research Center, Japan Atomic Energy Agency (SPring-8/JAEA), Sayo, Hyogo 679-5148, Japan. ⁴Institute for Solid State Physics, The University of Tokyo, Kashiwa, Chiba 277-8581, Japan. ⁵Department of Physics, The Chinese University of Hong Kong, Shatin, Hong Kong. ⁶Department of Physics, Kyoto University, Sakyo-ku, Kyoto 606-8502, Japan. ⁷Beijing National Laboratory for Condensed Matter Physics and Institute of Physics, Chinese Academy of Sciences, 100190 Beijing, China. Correspondence and requests for materials should be addressed to T.S. (email: shibauchi@k.u-tokyo.ac.jp)

One of the common aspects among unconventional superconductors, including high- T_c cuprates, heavy-fermion and organic materials, is the appearance of a superconducting dome in the vicinity of magnetic order. This has naturally led to the notion of superconducting pairing mechanism driven by magnetic fluctuations^{1,2}. In iron pnictides, high- T_c superconductivity also appears near the antiferromagnetic phase³, which however is accompanied by the tetragonal-to-orthorhombic structural transition with significant electronic anisotropy (nematicity). This gives rise to new theoretical proposals involving the fluctuations of this electronic nematicity as a glue for the electron pairing^{4–6}. Although enhanced nematic fluctuations of ferro-type ($q=0$) are observed experimentally⁷, the antiferromagnetic fluctuations are also enhanced⁸, and thus it is difficult to pinpoint the impact of nematic fluctuations on the superconductivity in iron pnictides.

From this viewpoint, the FeSe-based superconductors are a suitable system for addressing the importance of nematic fluctuations, as it has a unique phase diagram⁹. At ambient pressure, FeSe shows a nematic transition at $T_s=90$ K without magnetic order down to the lowest temperature¹⁰. Under pressure, antiferromagnetic order is induced^{11–16}, and the superconducting T_c is enhanced by more than a factor of 4^{9,17}. Recently, it has been shown that the nematic transition can be tuned to a quantum critical point by isovalent substitution of Se with S, but without inducing magnetic order¹⁸. These results indicate the non-equivalence of physical and chemical pressure in this system. This implies that one can control the magnetism and nematicity independently by these tuning knobs, isovalent substitution and physical pressure, which offers the possibility to disentangle intertwined effects of nematic and magnetic fluctuations on high- T_c superconductivity.

Here we present our systematic study of temperature-pressure-substitution (T - P - x) phase diagrams of $\text{FeSe}_{1-x}\text{S}_x$ in wide ranges of pressure (up to $P \sim 8$ GPa) and sulphur content ($0 \leq x \leq 0.17$). In pure FeSe, it has been shown by several groups that the nematic transition temperature T_s is suppressed by pressure ($P < 2$ GPa) but before the complete suppression of T_s , antiferromagnetic or spin density wave (SDW) order is induced, resulting in an overlap region of these two phases^{9,12–15}. With increasing x , the nematic transition temperature T_s is lowered and correspondingly the nematic phase is rapidly suppressed by pressure. However, an opposite trend is found for pressure-induced magnetism: the SDW onset pressure is shifted to higher pressure. These lead to the emergence of the tetragonal non-magnetic phase in between, which becomes wider with increasing x . Most importantly, a new high- T_c superconducting dome emerges in the tetragonal phase. Based on the obtained three-dimensional phase diagram, we discuss the relationship between the two orders and superconductivity in this system.

Results

Phase diagram. In $\text{FeSe}_{1-x}\text{S}_x$ at ambient pressure, the temperature dependence of resistivity $\rho(T)$ for $x < 0.17$ exhibits a slight upturn upon cooling at T_s due to tetragonal-to-orthorhombic structural transitions, and then it goes to zero below the superconducting transition temperature (T_c^{zero})¹⁸. By measuring $\rho(T)$, we determine the structural transition temperature (T_s) and (T_c^{zero}) for $x=0.04, 0.08$ and 0.12 at ambient pressure as shown in the electronic phase diagram for different S contents as shown in Fig. 1 (see also Supplementary Note 1, Supplementary Figs. 1, 2 for two-dimensional slices). For $x=0.17$, we do not observe any signature of the structural transition, indicating the complete

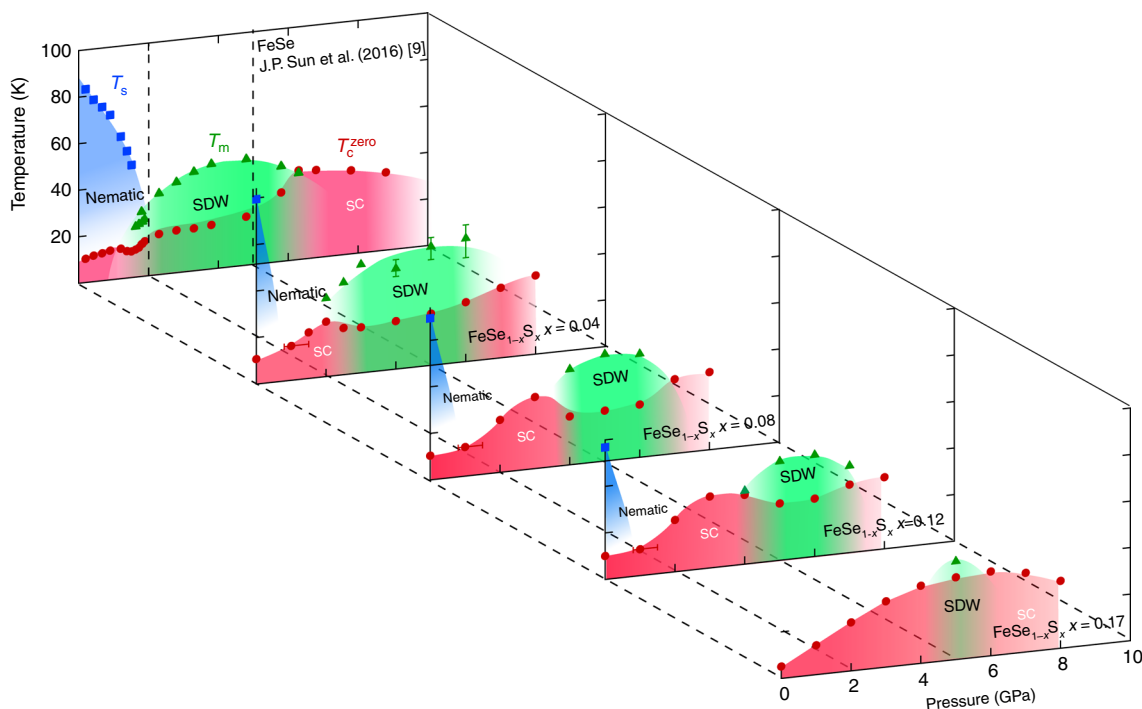


Fig. 1 Temperature-pressure-concentration phase diagram in $\text{FeSe}_{1-x}\text{S}_x$. The structural (T_s , blue squares), magnetic (T_m , green triangles) and superconducting transition temperatures (T_c^{zero} , red circles) are plotted against hydrostatic pressure P and S content x . Following the procedure reported for $x=0$ by Sun et al.⁹, T_s , T_m and T_c^{zero} are defined respectively by the temperatures of upturn, kink and zero resistivity in $\rho(T)$ curves measured in the constant-loading type cubic anvil cell for $x=0.04, 0.08, 0.12$ and 0.17 (Supplementary Figs. 3–6). The errors of T_m are estimated from the broadness of the kink anomaly in $\rho(T)$. The cell is optimized for the high-pressure range, and thus for $P < 2$ GPa the error of pressure is relatively large (see error bars for 1 GPa) compared to higher pressures. The colour shades are the guides for the eyes. Detailed phase diagrams for constant x and P are shown in Supplementary Figs. 1, 2, respectively

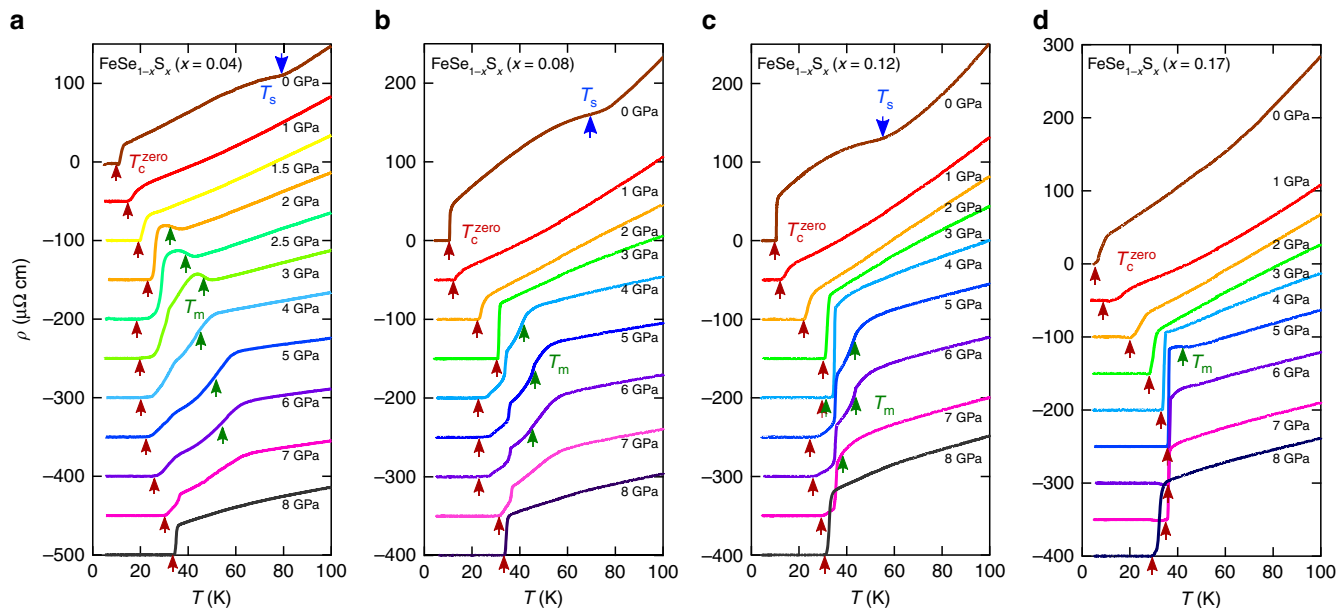


Fig. 2 Evolution of temperature-dependent resistivity under pressure in $\text{FeSe}_{1-x}\text{S}_x$. **a-d** $\rho(T)$ curves below 100 K at different pressures up to 8.0 GPa measured for $x = 0.04$ (**a**), 0.08 (**b**), 0.12 (**c**) and 0.17 (**d**). The data are vertically shifted for clarity. The resistive anomalies at transition temperatures T_s (blue), T_m (green) and T_c^{zero} (red) are indicated by the arrows. For $x = 0.04$ (**a**), the anomalies associated with the magnetic transition is smeared and thus the error of T_m determination is relatively large for $P \geq 4$ GPa (see error bars in Fig. 1)

suppression of T_s as reported previously¹⁸. In Fig. 2a–d, we show the evolution of $\rho(T)$ under pressure measured using a cubic anvil cell (CAC) which can generate pressure with a good hydrostatic condition and maintain constant pressure upon cooling¹⁹. With applying pressure, the T_s anomaly observed at ambient pressure in $x = 0.04$, 0.08 and 0.12 disappears completely at $P \lesssim 1$ GPa. This is a natural consequence of the fact that both S substitution and applying pressure suppress the structural transition in FeSe.

In $x = 0.04$, the $\rho(T)$ curve at 2.0 GPa exhibits a clear upturn around 40 K. The temperature of the upturn increases with pressure, and then it turns to a kink above 4.0 GPa. This evolution of resistive transition is reminiscent of the magnetic transition seen in FeSe under pressure⁹. Therefore, we follow the procedure of ref. ⁹ to determine the magnetic transition temperatures (T_m) by using a dip or peak in $d\rho/dT$ (Supplementary Note 2 and Supplementary Figs. 3–6), and the pressure-evolution of T_m is shown in Fig. 1 and Supplementary Fig. 1b. With increasing pressure, T_m is enhanced monotonically up to 6.0 GPa, while T_c^{zero} determined by the zero resistivity is slightly suppressed just after the emergence of magnetism. Inside the magnetic phase, the superconducting transition in $\rho(T)$ becomes broad. When we define T_c^{peak} as the peak temperature in $d\rho(T)/dT$ (Supplementary Fig. 3), the difference between T_c^{zero} and T_c^{peak} is significant in the magnetic phase (Supplementary Fig. 1). Above 7.0 GPa, the kink anomaly due to the magnetic transition disappears, and concomitantly T_c^{zero} increases gradually up to 32 K, resembling the evolution of the electronic phases in FeSe at high pressure⁹.

In $x = 0.08$ and 0.12, we observe remarkable features at moderate pressures. As shown in Fig. 2b, c, there is no discernible upturn anomaly in $\rho(T)$ between 1.0 and 3.0 GPa for $x = 0.08$ and 0.12. At 3.0 GPa, a clear T -linear behaviour in the normal-state resistivity is observed (Fig. 3b), which is accompanied by a sharp superconducting transition with enhanced T_c^{zero} of ~ 32 K. We checked for $x = 0.12$ that T_c determined by ac susceptibility is consistent with that determined by the zero resistivity (Supplementary Note 3, Supplementary Figs. 7, 8). Further increase of pressure leads to the emergence of magnetism seen as the kink

anomaly around 40 K, then it persists up to 6.0 (7.0) GPa for $x = 0.08$ (0.12). The marked difference compared with FeSe under pressure is the strong enhancement of T_c in the lower pressure side of the magnetic phase, forming a peak in T_c^{zero} around 3.0 GPa for both $x = 0.08$ and 0.12. With increasing pressure above 7.0 (8.0) GPa in $x = 0.08$ (0.12), the kink anomaly due to the magnetic transition disappears and T_c^{zero} exhibits another gradual enhancement up to ~ 32 K after the disappearance of T_m , resulting in the double-dome structure in T_c^{zero} having two maxima with almost identical magnitudes.

In $x = 0.17$, where there is no T_s at ambient pressure as shown in Fig. 2d, its initial T_c^{zero} of ~ 4 K gradually increases up to ~ 35 K with pressure, and turns to decrease above 6.0 GPa, forming a broad superconducting dome as a function of pressure as illustrated in Fig. 1. We observe T_m only at 5.0 GPa for this S content, implying that the system is approaching the verge of the pressure-induced SDW phase (Supplementary Fig. 2f).

Emergent tetragonal phase. As x is increased, the pressure-induced SDW dome shifts to higher pressure and shrinks, while low-pressure non-magnetic nematic phase shifts to lower pressure and disappears at $x \sim 0.17$. We stress that the nematic phase is completely separated from the SDW phase at $x \geq 0.04$. To confirm the separation between two distinct phases under pressure, we performed synchrotron X-ray diffraction measurements under pressure for $x = 0.08$ (Fig. 3a, and Supplementary Note 4). In Fig. 3b, c, we show (331) Bragg intensity as a function of temperature at 3.0 and 4.9 GPa together with the $\rho(T)$ and $d\rho/dT$ data. At 3.0 GPa, no discernible change of the Bragg-peak is observed down to the lowest temperature of 10 K (Fig. 3b and Supplementary Fig. 9a). At 4.9 GPa, on the other hand, the splitting of the Bragg peak is clearly resolved around $T_s \sim 41$ K, evidencing the presence of the tetragonal-to-orthorhombic structural transition (Fig. 3c and Supplementary Fig. 9b). This structural transition is located very close to the SDW transition at T_m at 5.0 GPa as indicated by the sharp peak in $d\rho/dT$ curve in Fig. 3b. Thus it is natural to consider that the magnetic phase has

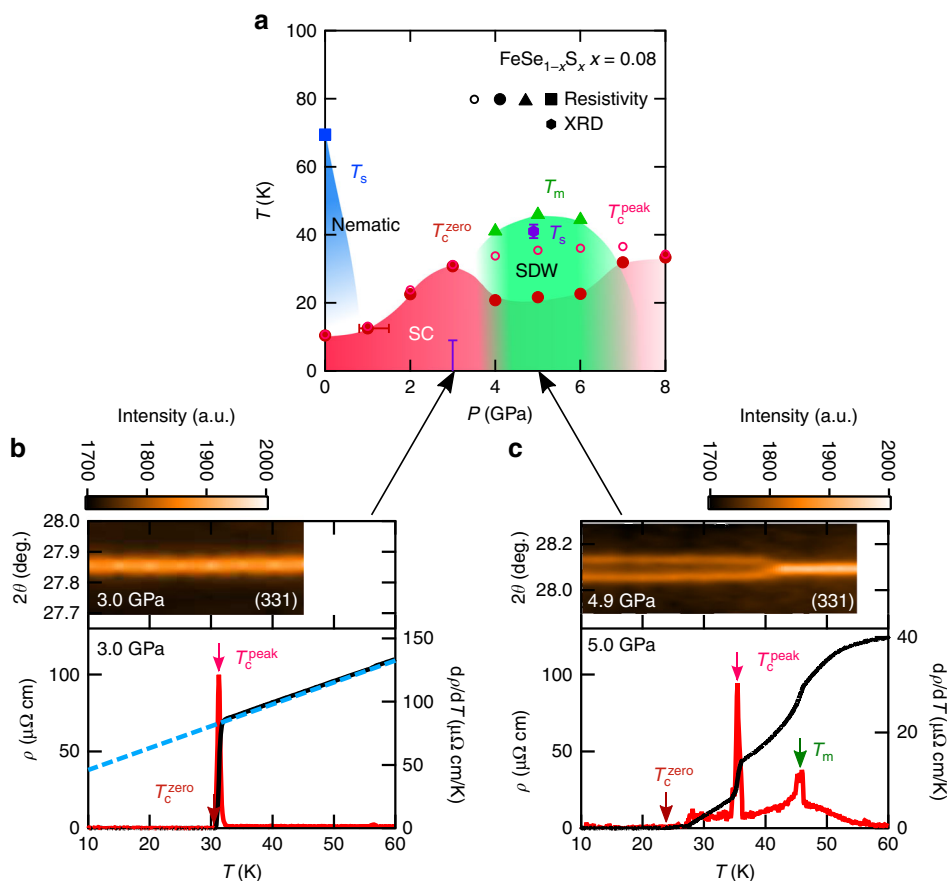


Fig. 3 Temperature-pressure phase diagram for $x = 0.08$. **a** T - P phase diagram of $\text{FeSe}_{1-x}\text{S}_x$ ($x = 0.08$) together with T_s determined by the high-pressure synchrotron X-ray diffraction (XRD) in a diamond anvil cell (purple hexagon with error bars). **b, c** Temperature dependence of Bragg intensity as a function of 2θ angle is indicated in colour scale for 3.0 GPa (**b**) and 4.9 GPa (**c**). $\rho(T)$ and $d\rho/dT$ are also shown with the same horizontal axis. The red, pink and green arrows indicate T_c^{zero} , T_c^{peak} and T_m , respectively. The blue dashed line in **b** is a T -linear fit to the normal-state $\rho(T)$ at 3.0 GPa

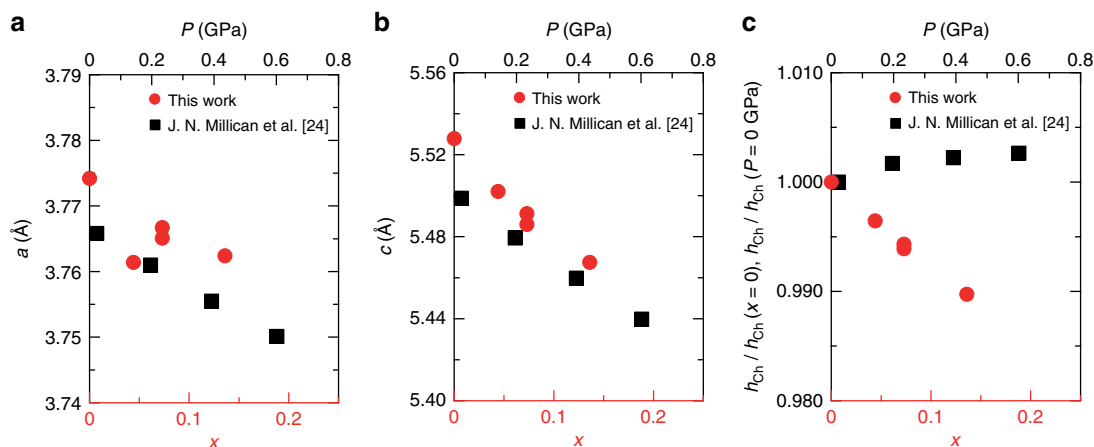


Fig. 4 Comparisons between physical pressure and isovalent substitution effects on the structural parameters. **a, b** Lattice constants a (**a**) and c (**b**) as a function of S content x in the present single crystals of $\text{FeSe}_{1-x}\text{S}_x$ (red circles, bottom axis), compared with those as a function of pressure reported for polycrystals of FeSe in ref. ²⁴ (black squares, top axis). **c** Chalcogen height h_{Ch} normalized by the initial values as a function of x (red circles, bottom axis) and pressure (black squares, top axis)²⁴. The numerical values of these parameters are listed in Supplementary Table 1

an orthorhombic structure, similar to the case of the high-pressure SDW phase of FeSe^{13,14}.

These results demonstrate that the high- T_c superconductivity in $\text{FeSe}_{1-x}\text{S}_x$ is realised in the tetragonal phase newly emerged

between the orthorhombic nematic and magnetic phases. In the non-magnetic tetragonal phase ($1 \text{ GPa} \lesssim P \lesssim 3 \text{ GPa}$), T_c shows a strong increase with P (Figs. 1, 3a), indicating that the enhancement of superconductivity is most pronounced near the

verge of the magnetic phase, not the nematic phase. It is also likely that the T -linear resistivity observed near the SDW boundary (Fig. 3b) is a consequence of enhanced antiferromagnetic fluctuations, as reported in other high- T_c cases^{8,20,21}.

Discussion

Why the effects of two tuning parameters, physical pressure and isovalent substitution, are so different? In general, applying pressure reduces lattice constants, and it leads to an increase of bandwidth as well as a change in the Coulomb interactions²², often affecting the ground state of the system. The chemical substitution by smaller ions also leads to a decrease of lattice constants, which results in similar effect on the system as the pressure effect. Indeed, in BaFe₂As₂ system, the physical and chemical pressure effects on superconductivity are essentially similar²³. To address the origin of the difference between chemical and physical pressure effects in FeSe, we determine the structure parameters of FeSe_{1-x}S_x at room temperature by single-crystal X-ray diffraction, which are compared with the published data under pressure²⁴ (Fig. 4a–c and Supplementary Table 1). As expected, both a -axis and c -axis lattice constants decrease with S content x , which follow the trends under physical pressure. The quantitative comparison suggests that 10% substitution corresponds to ~ 0.3 GPa (Fig. 4a, b). This can be compared with effects of chemical and physical pressure on the phase diagrams of BaFe₂As₂, where the 30% substitution of P for As²¹ and application of ~ 0.55 GPa²⁵ both lead to the maximum $T_c \sim 30$ K.

In sharp contrast to the a -axis and c -axis lattice constants, there is a significant difference in the trends of the chalcogen height h_{Ch} from the iron plane (Fig. 4c). It has been pointed out in iron pnictides that the height of the anion atoms from the Fe plane plays an important role on the existence of hole-like Fermi surface around the zone corner of the unfolded Brillouin zone, which has significant influence on the nesting properties between the Fermi surfaces²⁶. It has also been shown that the chalcogen height in FeSe_{1-x}Te_x is an important factor for the magnetic interactions²⁷. We find that the isovalent substitution reduces h_{Ch} monotonically which is opposite to the observed increasing trend due to physical pressure effect. Thus, this contrasting variation of the chalcogen height against chemical and physical pressures is likely responsible for the shift of the magnetic dome to the higher pressure side with S-substitution, because for samples with a larger S content a higher pressure is required for obtaining a large enough h_{Ch} to induce magnetic order. Indeed, recent theoretical calculation investigating the pressure effect in FeSe points out that the increase of h_{Ch} results in the appearance of Fermi surface in the Brillouin zone corner, which explains the emergence of magnetism under pressure²⁸.

Another intriguing observation is that inside the SDW phase the superconducting transition becomes broad with a relatively high onset temperature (Fig. 2 and Supplementary Figs. 3–6). This is demonstrated in Supplementary Fig. 1, which shows that T_c^{peak} defined by the peak temperature in $d\rho(T)/dT$ continues to rise with pressure upon entering the SDW phase, whereas the zero resistivity T_c^{zero} is suppressed. This implies the competing nature of the magnetic and superconducting orders, which may disturb the development of high- T_c superconductivity. Indeed, a recent detailed study of ac susceptibility measurements under pressure shows that the volume fraction in the diamagnetic shielding is suppressed in the pressure-induced SDW phase, pointing to non-bulk superconductivity inside the magnetic phase²⁹.

We have shown that by combining physical and chemical pressure effects, which can change the chalcogen height in different manners, nematicity and magnetism can be tuned to

control T_c in FeSe-based superconductors. The most notable feature is that the high- T_c superconductivity in the tetragonal phase emerges at the verge of both side of the SDW dome, while T_c is little influenced by the non-magnetic nematic phase. Magnetic order appears to exert two effects on superconductivity: on one hand, their competing nature suppresses the formation of bulk high- T_c superconductivity inside the magnetic phase, and on the other hand, the enhanced fluctuations near the end points of the magnetic phase may help increase T_c , much more significant than the non-magnetic fluctuations near the nematic quantum critical point at $x \sim 0.17$ and $P \sim 0$ GPa. In view of the orthorhombicity found in the pressure-induced SDW phase, an intriguing issue that deserves further studies is whether the nematic and magnetic fluctuations cooperatively promote the superconducting pairing, as recently suggested theoretically²⁸.

Methods

Single crystals. High-quality single crystals of FeSe_{1-x}S_x ($x = 0, 0.04, 0.08, 0.12$ and 0.17) have been grown by the chemical vapour transport technique¹⁸. The x values are determined by the energy dispersive X-ray spectroscopy. In the crystals obtained under identical conditions, quantum oscillations have been observed in a wide range of $x (\leq 0.19)$ ³⁰, indicating superior crystal quality.

High-pressure measurements. High-pressure resistivity $\rho(T, P)$ measurements have been performed under hydrostatic pressures up to 8 GPa with a constant-loading type cubic anvil apparatus which can maintain a nearly constant pressure over the whole temperature range from 300 to 2 K^{9,19}. For all these high-pressure resistivity measurements, we employed glycerol as the pressure-transmitting medium, and used the conventional four-terminal method with current applied within the ab plane. High-pressure ac susceptibility measurements have been done by using a mutual inductance technique in a moissanite anvil cell with glycerol as the pressure-transmitting medium²³. The pressure achieved was determined by measuring the wavelength of the R_1 peak of ruby fluorescence. Synchrotron X-ray diffraction measurements under pressure have been performed at BL22XU in SPring-8 by using diamond anvil cell diffractometer equipped with a gas membrane for maintaining constant pressure on cooling³¹. Helium is used as the pressure-transmitting medium. The pressure value in the sample space is monitored by tracking the ruby fluorescence wavelength for the whole temperature range.

Data availability. The data that support the findings of this study are available from the corresponding author upon reasonable request.

Received: 27 April 2017 Accepted: 4 September 2017

Published online: 26 October 2017

References

- Moriya, T. & Ueda, K. Spin fluctuations and high temperature superconductivity. *Adv. Phys.* **49**, 555–606 (2000).
- Monthoux, P., Pines, D. & Lonzarich, G. G. Superconductivity without phonons. *Nature* **450**, 1177–1183 (2007).
- Fernandes, R. M., Chubukov, A. V. & Schmalian, J. What drives nematic order in iron-based superconductors? *Nat. Phys.* **10**, 97–104 (2014).
- Maier, T. A. et al. Pairing interaction near a nematic quantum critical point of a three-band CuO₂ model. *Phys. Rev. B* **90**, 174510 (2014).
- Lederer, S. et al. Enhancement of superconductivity near a nematic quantum critical point. *Phys. Rev. Lett.* **114**, 097001 (2015).
- Kontani, H. & Onari, S. Orbital-fluctuation-mediated superconductivity in iron pnictides: Analysis of the five-orbital Hubbard-Holstein model. *Phys. Rev. Lett.* **104**, 157001 (2010).
- Böhmer, A. E. & Meingast, C. Electronic nematic susceptibility of iron-based superconductors. *Compt. Rend. Phys.* **17**, 90–112 (2016).
- Shibauchi, T., Carrington, A. & Matsuda, Y. A quantum critical point lying beneath the superconducting dome in iron-pnictides. *Ann. Rev. Condens. Matter Phys.* **5**, 113–135 (2014).
- Sun, J. P. et al. Dome-shaped magnetic order competing with high-temperature superconductivity at high pressures in FeSe. *Nat. Commun.* **7**, 12146 (2016).
- Baek, S.-H. et al. Orbital-driven nematicity in FeSe. *Nat. Mater.* **14**, 210–214 (2015).
- Bendele, M. et al. Pressure induced static magnetic order in superconducting FeSe_{1-x}. *Phys. Rev. Lett.* **104**, 087003 (2010).

12. Terashima, T. et al. Pressure-induced antiferromagnetic transition and phase diagram in FeSe. *J. Phys. Soc. Jpn* **84**, 063701 (2015).
13. Kothapalli, K. et al. Strong cooperative coupling of pressure-induced magnetic order and nematicity in FeSe. *Nat. Commun.* **7**, 12728 (2016).
14. Wang, P. S. et al. Pressure induced stripe-order antiferromagnetism and first-order phase transition in FeSe. *Phys. Rev. Lett.* **117**, 237001 (2016).
15. Kaluarachchi, U. S. et al. Nonmonotonic pressure evolution of the upper critical field in superconducting FeSe. *Phys. Rev. B* **93**, 064503 (2016).
16. Terashima, T. et al. Magnetotransport study of the pressure-induced antiferromagnetic phase in FeSe. *Phys. Rev. B* **93**, 180503 (2016).
17. Medvedev, S. et al. Electronic and magnetic phase diagram of β -Fe_{1-x}S_x with superconductivity at 36.7 K under pressure. *Nat. Mater.* **8**, 630 (2010).
18. Hosoi, S. et al. Nematic quantum critical point without magnetism in FeSe_{1-x}S_x superconductors. *Proc. Natl Acad. Sci. USA* **113**, 8139–8143 (2016).
19. Mori, N., Takahashi, H. & Takeshita, N. Low-temperature and high-pressure apparatus developed at ISSP, University of Tokyo. *High Press. Res.* **24**, 225–232 (2004).
20. Sun, J. P. et al. High- T_c superconductivity in FeSe at high pressure: dominant hole carriers and enhanced spin fluctuations. *Phys. Rev. Lett.* **118**, 147004 (2017).
21. Kasahara, S. et al. Evolution from non-Fermi- to Fermi-liquid transport via isovalent doping in BaFe₂(As_{1-x}P_x)₂ superconductors. *Phys. Rev. B* **81**, 184519 (2010).
22. Scherer, D. D. et al. Interplay of nematic and magnetic orders in FeSe under pressure. *Phys. Rev. B* **95**, 094504 (2017).
23. Klintberg, L. E. et al. Chemical pressure and physical pressure in BaFe₂(As_{1-x}P_x)₂. *J. Phys. Soc. Jpn* **79**, 123706 (2010).
24. Millican, J. N., Phelan, D., Thomas, E. L., Leão, J. B. & Carpenter, E. Pressure-induced effects on the structure of the FeSe superconductor. *Solid State Commun.* **149**, 707–710 (2009).
25. Colombier, E., Bud'ko, S. L., Ni, N. & Canfield, P. C. Complete pressure-dependent phase diagrams for SrFe₂As₂ and BaFe₂As₂. *Phys. Rev. B* **79**, 224518 (2009).
26. Kuroki, K. et al. Pnictogen height as a possible switch between high- T_c nodeless and low- T_c nodal pairings in the iron-based superconductors. *Phys. Rev. B* **79**, 224511 (2009).
27. Moon, C.-Y. & Choi, H. J. Chalcogen-height dependent magnetic interactions and magnetic order switching in FeSe_{1-x}Te_x. *Phys. Rev. Lett.* **104**, 057003 (2010).
28. Yamakawa, Y. & Kontani, H. Nematicity, magnetism and superconductivity in FeSe under pressure: Unified explanation based on the self-consistent vertex correction theory. Preprint at <https://arxiv.org/abs/1609.09618>.
29. Yip, K. Y. et al. Weakening of the diamagnetic shielding in FeSe_{1-x}S_x at high pressures. *Phys. Rev. B* **96**, 020502 (2017).
30. Coldea, A. I. et al. Evolution of the Fermi surface of the nematic superconductors FeSe_{1-x}S_x. Preprint at <https://arxiv.org/abs/1611.07424>.
31. Watanuki, T. et al. Development of a single-crystal X-ray diffraction system for hydrostatic-pressure and low-temperature structural measurement and its application to the phase study of quasicrystals. *Philos. Mag.* **87**, 2905–2911 (2007).

Acknowledgements

We thank H. Kontani and Y. Yamakawa for fruitful discussions. We also thank S. Nagasaki and T. Watashige for technical assistance. This work was performed using facilities of the Institute for Solid State Physics, the University of Tokyo. A part of this

work was performed under the Shared Use Program of JAEA and QST Facilities (Proposal No. 2015A-E16, 2016A-E16, and 2016B-H13) supported by JAEA, QST Advanced Characterization Nanotechnology Platform as a program of “Nanotechnology Platform” of the Ministry of Education, Culture, Sports, Science and Technology (MEXT), Japan (Proposal No. A-15-AE-0016, A-16-QS-0008, and A-16-QS-0025). The synchrotron radiation experiments were performed by using a QST experimental station at JAEA beamline BL22XU in SPring-8 with the approval of the Japan Synchrotron Radiation Research Institute (JASRI) (Proposal No. 2015A3701, 2015A3783, 2015B3701, 2016A3751, 2016A3781 and 2016B3785). This work was supported by Grant-in-Aids for Scientific Research (A), (B), (S), (Proposal No. 15H02106, 15H03681, 15H03688, and 25220710) and Grant-in-Aid for Young Scientists (B) (Proposal No. 15K17692) from Japan Society for the Promotion of Science (JSPS), Grant-in-Aids on Innovative Areas “Topological Materials Science” (No. 15H05852) from MEXT, CUHK Startup Grant (No. 4930048), and Research Grant Council of Hong Kong (ECS/24300214, GRF/14301316). J.-G.C. acknowledges the supported from the NSFC, MOST, and CAS (Proposal No. 11574377, 2014CB921500, XDB07020100 and QYZDB-SSW-SLH013).

Author contributions

T.S. conceived the project. K. Matsuura, Y.A., Y.S., J.-G.C. and Y.U. measured the resistivity under pressure using CAC. K. Matsuura, Y. Mizukami, N.M., A.M., T.W., T.F., S.H., K.I. and S.K. performed high-pressure X-ray diffraction measurements. Y. Mizukami, T.Y. and Z.H. performed X-ray diffraction measurements for FeSe_{1-x}S_x at ambient pressure. K.Y.Y., Y.C. C., Q.N. and S.K.G. measured the susceptibility under pressure. K. Matsuura, K. Mukasa, S. K. and Y. Matsuda synthesized FeSe_{1-x}S_x single crystals. All authors discussed the results. K. Matsuura, Y. Mizukami, Y. Matsuda, T.S. wrote the paper with inputs from all authors. Y. Matsuda, Y.U. and T.S. supervised the projects.

Additional information

Supplementary Information accompanies this paper at doi:10.1038/s41467-017-01277-x.

Competing interests: The authors declare no competing financial interests.

Reprints and permission information is available online at <http://npg.nature.com/reprintsandpermissions/>

Publisher's note: Springer Nature remains neutral with regard to jurisdictional claims in published maps and institutional affiliations.



Open Access This article is licensed under a Creative Commons Attribution 4.0 International License, which permits use, sharing, adaptation, distribution and reproduction in any medium or format, as long as you give appropriate credit to the original author(s) and the source, provide a link to the Creative Commons license, and indicate if changes were made. The images or other third party material in this article are included in the article's Creative Commons license, unless indicated otherwise in a credit line to the material. If material is not included in the article's Creative Commons license and your intended use is not permitted by statutory regulation or exceeds the permitted use, you will need to obtain permission directly from the copyright holder. To view a copy of this license, visit <http://creativecommons.org/licenses/by/4.0/>.

© The Author(s) 2017